Engineering Structures

Subsea Pipeline Defect Mapping: A Bold and Successful Attempt Based on Dry Cabin and Structured Light
--Manuscript Draft--

Manuscript Number:	ENGSTRUCT-D-24-02187
Article Type:	Research Paper
Section/Category:	Oceania, Mainland China, Taiwan, Hong Kong, Macau, Singapore, Japan, Korea
Keywords:	subsea pipeline, precise defect scanning, dry cabin, structured light
Corresponding Author:	Jiawang Chen Donghai laboratory CHINA
First Author:	Hai Zhu
Order of Authors:	Hai Zhu
	Yuan Lin
	Zhangyong Jin
	Jin Guo
	Jiawang Chen
	Han Ge
	Kaichuang Wang
	Peiwen Lin
	Haonan Li
	Xiaoqing Peng
	Peng Zhou
	Yuping Fang
	Xueyu Ren
	Yuhong Wang
	Yongqiang Ge
	Xuehua Chen
	Xu Gao
	Yuanjie Chen
Manuscript Region of Origin:	Asia Pacific
Abstract:	Subsea pipelines play a crucial role in the transportation of offshore oil and gas, yet they are susceptible to deformation defects over time due to various marine factors, posing significant threats to their safety and integrity. Conventional acoustic and electromagnetic detection methods often fall short in accurately scanning for defects, particularly in harsh sea conditions with high turbidity. This research focuses on the integration of dry cabin and structured light technology to design, simulate, and validate the effectiveness of core dry cabin sealing and high-pressure gas purging for media transfer. Additionally, a structured light scanning system is developed, analyzed in principle, and validated through sea trials, enabling precise external mapping of underwater pipelines. The obtained editable point cloud data and extracted dimensional parameters facilitate the evaluation of damage severity and risk coefficients for subsea pipelines, thereby aiding in the formulation of targeted repair strategies. Consequently, this study represents a valuable enhancement to existing subsea pipeline defect detection technologies, offering a more comprehensive approach to assessing and mitigating risks in offshore operations.

Suggested Reviewers:	Yongping Jin Hunan University of Science and Technology jinyongping12@163.com I would like to recommend Professor Jin as a potential reviewer for this paper due to his extensive expertise and profound contributions in the field of ocean engineering equipment development.
	Guang Pan Northwestern Polytechnical University panguang@nwpu.edu.cn With a longstanding commitment to research in this area, Professor Pan possesses a wealth of knowledge and experience that make him well-suited to provide valuable insights and constructive feedback on the manuscript. His deep understanding of subsea technologies and their practical applications ensures that his review will be thorough and informed. Additionally, Professor Pan's stature in the field lends credibility to the peer review process, further enhancing the quality and impact of the publication.
Opposed Reviewers:	

Dear Editors,

Enclosed, please find our submission entitled "Subsea Pipeline Defect Mapping: A Bold and Successful Attempt Based on Dry Cabin and Structured Light" for consideration for publication in 《Engineering Structures》. This study delves into the defect mapping technology of subsea pipelines, presenting a novel approach that utilizes dry cabin and structured light technology, yielding promising results.

Our article outlines the key implementation methods, including an explanation of the working principles behind seal, medium displacement, and structured light mapping. Additionally, we provide detailed insights into the calculations, methodologies, results, and discussions derived from our research.

We, the co-authors, confirm our substantial contribution to the work, ensuring accountability for the experimental design, methodology, data collection, analysis, and interpretation. Having thoroughly reviewed the final version of the manuscript, we collectively endorse its readiness for publication. Furthermore, we affirm that this manuscript has not been previously published, nor is it under consideration elsewhere.

Thank you for considering our submission.

Yours Sincerely,
Hai Zhu, Yuan Lin, Zhangyong Jin, Jin Guo, Jiawang Chen, Han Ge, Kaichuang Wang, Peiwen Lin, Haonan Li, Xiaoqing Peng, Peng Zhou, Yuping Fang, Xueyu Ren, Yuhong Wang, Yongqiang Ge, Xuehua Chen, Xu Gao, Yuanjie Chen

Highlights

- Utilization of foam EPDM for adaptive sealing instead of rigid rubber

- The successful construction of a dry cabin guided by hyperbaric gas inflation theory

- Innovative application of structured light technology in subsea pipeline inspection

- Provision of a comprehensive solution for the scanning driving and its scan strategy

- Attainment of remarkable accuracy even under demanding marine conditions

Declaration of interests

☐The authors declare that they have no known competing financial interests or personal relationships that could have appeared to influence the work reported in this paper.

☒The authors declare the following financial interests/personal relationships which may be considered as potential competing interests:

Subsea Pipeline Defect Mapping: A Bold and Successful Attempt Based on Dry Cabin and Structured Light

Hai Zhu[a], Yuan Lin[a], Zhangyong Jin[a], Jin Guo[a], Jiawang Chen[a,b,*], Han Ge[a], Kaichuang Wang[a], Peiwen Lin[a], Haonan Li[a], Xiaoqing Peng[a], Peng Zhou[a], Yuping Fang[a], Xueyu Ren[a], Yuhong Wang[a], Yongqiang Ge[a], Xuehua Chen[c], Xu Gao[a,c], Yuanjie Chen[d]

[a] Institute of Ocean Engineering and Technology, Zhejiang University, Zhoushan, Zhejiang 316021, China

[b] Donghai Laboratory, Zhoushan, Zhejiang 316021, China

[c] Pipe China Eastern Oil Storage and Transportation Co. Ltd., ZhouXu, Jiangsu 221008, China

[d] Zhejiang Province Institute of Metrology, Hangzhou, Zhejiang 310063, China

* Corresponding author. E-mail: arwang@zju.edu.cn, Tel: +8618667171179, Fax: 0580-2092214, Address: 101 Haigong Building, Zhoushan Campus, Zhejiang University, Dinghai District, Zhoushan City, Zhejiang Province, China

ABSTRACT Subsea pipelines play a crucial role in the transportation of offshore oil and gas, yet they are susceptible to deformation defects over time due to various marine factors, posing significant threats to their safety and integrity. Conventional acoustic and electromagnetic detection methods often fall short in accurately scanning for defects, particularly in harsh sea conditions with high turbidity. This research focuses on the integration of dry cabin and structured light technology to design, simulate, and validate the effectiveness of core dry cabin sealing and high-pressure gas purging for media transfer. Additionally, a structured light scanning system is developed, analyzed in principle, and validated through sea trials, enabling precise external mapping of underwater pipelines. The obtained editable point cloud data and extracted dimensional parameters facilitate the evaluation of damage severity and risk coefficients for subsea pipelines, thereby aiding in the formulation of targeted repair strategies. Consequently, this study represents a valuable enhancement to existing subsea pipeline defect detection technologies, offering a more comprehensive approach to assessing and mitigating risks in offshore operations.

KEYWORDS subsea pipeline, precise defect scanning, dry cabin, structured light.

1. Introduction

The ocean is commonly referred to as the "blue frontier" [1]due to its abundance of resources, which include, but are not limited to, minerals, biological organisms, and water resources. Among these resources, energy minerals, such as oil, gas, and gas hydrates, are particularly important in subsea formations[2]. The conventional approach for exploiting offshore oil and gas resources involves drilling platforms extracting oil and gas from subsea formations and using subsea pipelines to transport the resources to land-based refineries.

Subsea pipelines trace their origin to the Gulf of Mexico[3], where the world's first subsea pipeline was constructed in 1954. Chinese inaugural subsea pipeline was successfully laid in Huangdao, Shandong, in 1973. With the development of national industrialization, the demand for oil and gas transportation has further expanded, and remarkable strides in national construction capabilities have provided practical underpinnings for cross-sea subsea pipelines. The length of subsea pipelines has experienced phenomenal growth, endowing offshore oil and gas exploitation with robust capacity. However, the concomitant expansion of subsea pipeline installations has also escalated maintenance difficulties, risk factors, and costs.

Subsea pipelines are a vital lifeline for offshore oil-gas fields[4,5], playing a crucial role in their development, production, and transportation. On the one hand, severe damage or leakage of subsea pipelines can disrupt energy supplies, causing significant economic losses to companies and countries. On the other hand, damage and leakage can also result in severe pollution in the surrounding marine environment, leading to ecological disasters. To ensure the safety of subsea pipelines in different application scenarios, the structural design of subsea pipelines has become increasingly complex and specialized over the past few decades, with various types such as single-layer steel pipe, double-layer insulated steel pipe, internally clad alloy steel pipe, flexible pipe, and bundled pipeline[6–8]. The evolution of structural forms of subsea pipelines reflects that the marine environment destroys the pipeline in a wide range of forms (including corrosion[9–11], reciprocating current scouring[12,13], seabed liquefaction[14], anchorage operation, etc.) and induces each other. Cross-aggravation occurs from time to time. Some particular reasons will also cause the destruction of subsea pipelines (the Nord Stream Subsea Pipelines[15], shown in fig1), which will have a far-reaching impact on social production, human livelihoods, and the ecological environment.

The demand for accurately identifying the location and extent of damage in subsea pipeline systems has increased in recent years, leading to a consensus within the industry to develop defect inspection technology for subsea pipelines. This development has primarily branched into two directions: internal inspection and external inspection. Currently, subsea pipeline internal inspection is the predominant technology employed due to its diverse technical forms, convenient scanning and scanning capabilities, and relatively low cost[16]. However, the unique requirements of subsea pipelines necessitate inspection equipment that should be highly passability because the repair costs associated with blockages can be prohibitively high. Furthermore, subsea pipeline internal inspection suffers from limitations such as poor positioning accuracy, challenging speed control, and inadequate data point resolution, which constrains its utility. Consequently, developing subsea pipeline external inspection technology represents an important supplement to existing subsea pipeline defect inspection technology.

Fig. 1. Schematic diagram and photos of damaged points of the Nord Stream pipeline

Subsea pipeline external inspection technologies can generally be classified into geophysical exploration and diving inspection methods. The former includes the use of equipment and techniques such as sub-bottom profilers (SBP), multibeam systems (MBS), side-scan sonar systems (SSS), and magnetic anomaly detectors (MAD) for conventional external inspection of subsea pipelines[17–19]. The latter involves underwater inspections carried out by divers or remotely operated vehicles (ROVs), with primary methods including underwater visual inspections (UWVI), contact point inspections(CPI)[20], ultrasonic testing (UT)[21], eddy current testing (ECT)[22], magnetic flux leakage (MFL)[23], alternating current field measurement (ACFM), and radiographic inspections (RT)[24]. However, When used in isolation, the current state-of-the-art technology of acoustic and electromagnetic detection methods fails to adequately fulfill the demand for quantitatively characterizing defects, providing high scanning precision, facilitating ease of transportation, and operating under harsh sea conditions in subsea pipelines. While optical detection methods offer superior solutions to these issues[25–32], their applicability is often restricted by the peculiarities of the seabed environment, notably, the interference from seawater.

After a thorough investigation, this study has revealed that conventional pipeline inspection methods are incapable of generating comprehensive and accurate 3D models of subsea pipelines, mainly due to two primary obstacles: the hindrance caused by highly turbid seawater and the requirement for exceptional precision. To address these challenges, we have adopted a fresh approach by targeting dry cabins designed for underwater use, which can enable high-precision scanning equipment that was not initially intended for subsea applications. Our research has shown that in China, only one dry cabin is available for non-submerged pipeline repairs[33], and there are no documented instances of dry scanning cabins for pipelines at depths exceeding 30 meters. The technical details of the Deepwater Pipeline Repair System (DPRS) developed by DCN in the Netherlands are not publicly accessible. It lacks scanning capabilities, necessitating personnel to work in a high-pressure airlock. Nautilus is the world's -first subsea pipeline repair robot developed by ARV and Kongsberg Ferrotech. It saves pipeline spot repair operating costs by innovatively completing subsea pipeline maintenance tasks twice faster as conventional saturation divers' repairs without compromising safety and quality. The Nautilus utilizes an open half-cabin for repairing pipelines but does not include scanning capabilities. Although neither of these overseas devices has scanning capabilities, they have successfully formed dry cabins underwater, inspiring our research.

2. System Design

2.1. Overall structure design

The target of the survey equipment at hand is the subsea pipelines connecting Zhoushan and Ningbo, which have been designed to withstand various environmental factors before laying. The pipeline is coated with a concrete weight coating, an epoxy layer, and a Bellota anti-corrosion layer to ensure sufficient anti-corrosion ability and structural strength. Despite these measures, the pipeline has suffered from partial joint damage over the course of several years. In 2017, The first party conducted an internal inspection using existing technologies. They identified severe deformation in the pipeline at some points. However, the lack of measurement accuracy prevented the development of corresponding repair plans. Given the nature of subsea pipeline defects, the survey equipment adopted must satisfy the following requirements:

1. The measured length of the pipeline must be≥5 meters.
2. The measurement accuracy must be ≤1mm.
3. Maximum applicable water depth: 30 meters.
4. It must be suitable for subsea pipelines with a diameter of 762mm and capable of forming adaptive seals for pipelines with bending angles of up to 15 degrees.
5. It must be able to produce a 3D editable data model within 6 hours.
6. The resulting 3D data model must be of high accuracy and editable. All data must adhere to relevant standards and requirements, ensuring the accuracy and reliability of the scanning results.
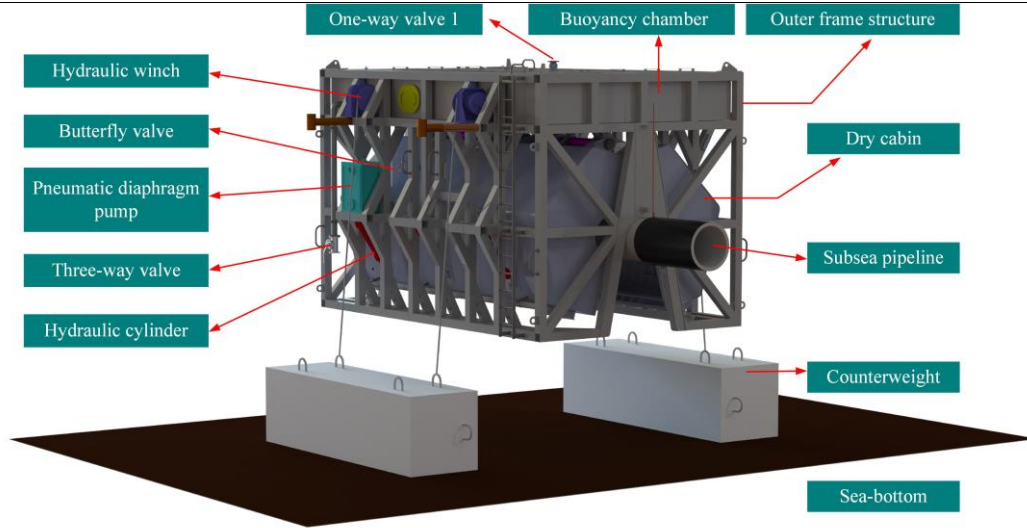
2

Fig. 2. Overall struture of subsea pipeline mapping device

The configuration of the subsea pipeline defect mapping device, depicted in Figure 2, deviates from conventional technical approaches by establishing mapping conditions for underwater structural defect detection using a dry cabin. The integration of structured light technology significantly enhances mapping precision (up to 0.1mm). The core structure of the mapping device comprises a dry cabin, characterized by a regular hexagonal cross-sectional shape, considering factors such as upstream face dimensions, flow resistance coefficient, internal wiring installation, cabin volume, and opening/closing mechanisms. Supplementary components crucial for functionality include hydraulic winches, adjustable buoyancy chamber, outer frame structure, hydraulic cylinders, counterweights, one-way valves, three-way valve, pneumatic diaphragm pumps, etc., positioned as indicated in Figure 2. Additionally, non-core structures and equipment encompass high-pressure air ports, liquid level sensors, lifting lugs, drainage pipelines, valves, steel wire ropes, etc., although these are not detailed herein.

2.2. Seal design for dry cabin

The key to the formation of the dry cabin lies in the ability of its seal to form and maintain stability over the long term, making the design of the dry cabin seal structure paramount. To minimize diver intervention and thereby enhance operational efficiency, the seal form and structure necessitate simplicity and effectiveness. To facilitate the wrapping and detachment of the pipeline, it is designed as two semi-cabins that close and dock to achieve sealing. The opening and closing of the dry cabin are executed by hydraulic cylinders and remotely controlled by onboard personnel. The seal structure is simplified by embedding the sealing rubber into U-shaped steel grooves, facilitating the replacement of the sealing rubber.

While using hard rubber for sealing is a common technique, its limited adjustability range leaves little room for adaptation to the uneven surfaces of subsea pipelines and the dry cabin. Therefore, foam sealing rubber is employed at the ends of the dry cabin. As depicted in Figure 3, the end structure is complex, particularly involving the annular sealing surface with the pipeline. Hence, the sealing strip is processed and assembled in segments. The challenge of sealing the upper and lower surfaces of the dry cabin lies in the differing sealing strokes before and after cabin closure. The upper seal stroke is short and does not require adaptive sealing with defect structures, thus hard rubber is used. Conversely, the lower seal stroke necessitates adaptability and utilizes foam rubber.
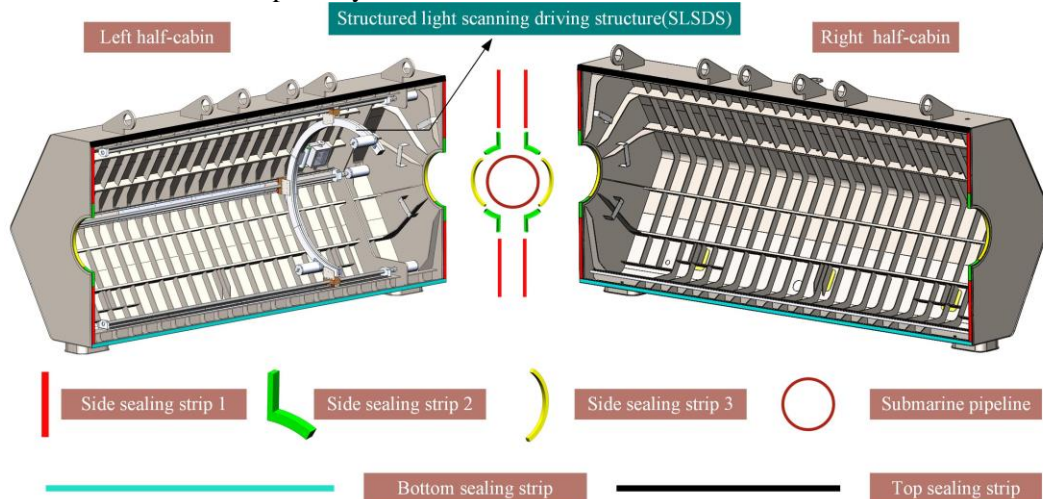

Fig. 3. Overall struture of subsea pipeline mapping device

3

2.2. Medium displacement system(MDS)

As shown in Figure 4, the primary methodology employed by MDS to establish a dry cabin entails the utilization of a pneumatic blowing subsystem (PBS) in conjunction with pumps for water drainage. The PBS, employing an air compressor as its air source, operates in tandem with pipelines and valves to effectuate high-pressure air blowing for seawater expulsion within the dry cabin. Traditionally employed in submarines, the PBS functions by gradually introducing high-pressure gas into the dry cabin, thereby increasing internal pressure to balance with external water pressure, and expelling water to the buoyancy chamber until the dry cabin is devoid of water. The depth of the surrounding water determines the hyperbaric gas pressure within the dry cabin, necessitating a specific pressure differential to ensure an effective seal between the cabin and seawater. Due to the diminished efficacy of high-pressure air blowing in later stages, submersible pumps are employed for seawater suction to enhance displacement efficiency and establish a successful dry environment. Complementarily, two pneumatic diaphragm pumps are utilized to supplement and substitute the submersible pump when it operates without submersion. The buoyancy chamber design accommodates a portion of transferred cabin water, mitigating buoyancy values generated by drainage. Furthermore, to constrain the buoyancy effects on subsea pipelines post-drainage, a hydraulic winch is engaged to tension the steel wire rope connecting the outer frame structure with counterweights, thereby achieving suspension of the entire device and minimizing its impact on seabed pipelines.
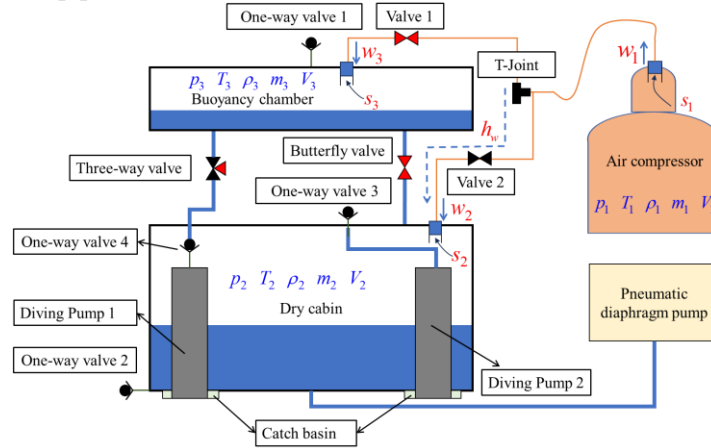

Fig. 4. Schematic diagram of medium displacement system[34]

2.3. Structured light scanning system(SLSS)

The subsea pipeline defect mapping based on the dry cabin and structured light mainly consists of a structured light scanning driving structure (SLSDS) and shipboard electrical control system. As shown in Figure 5, the SLSDS consists of motors, scanners, seal chambers, circular orbit, slide rails, and so on. After the establishment of the dry cabin, the SLSDS drives a structured light scanner to perform a 360° scan around the pipeline while ensuring axial motion within a 5m range, which is pre-designed and equipped inside the dry cabin. The position change of the scanner is achieved by three drive modules(straight-rail drive module, ring-track drive module, and angle drive module), which cooperate with the gears to achieve three fundamental functions: axial linear motion, circumferential rotational motion, and small angle adjustment motion.
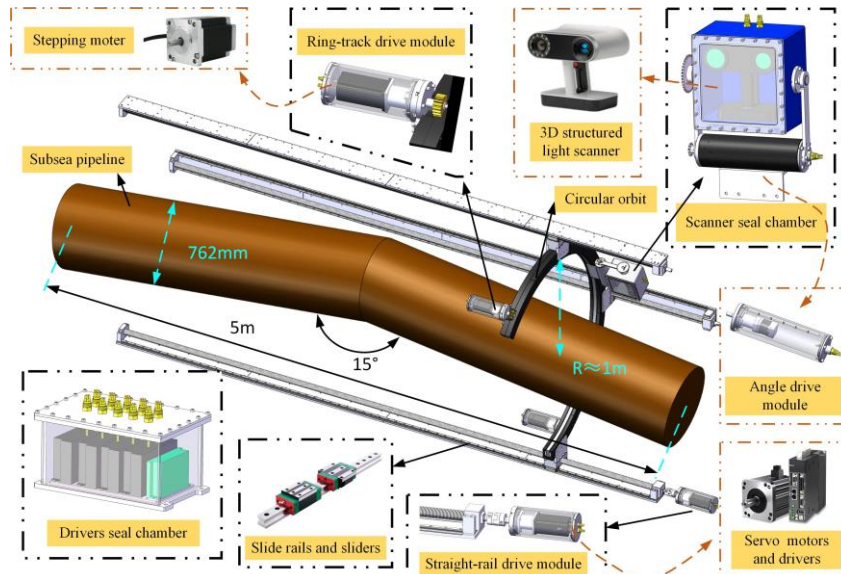

Fig. 5. Structured light scanning driving structure

4

The propulsion system of the motor relies on the shipboard electrical control system. Its fundamental principle involves utilizing an upper computer to send and receive commands, modulating signals through an optical transceiver, converting them into optical signals, and transmitting them to the motor driver. The power supply for the motor is centrally controlled through a distribution cabinet. The accurate issuance of commands depends on the collection of various data inside the underwater dry cabin, including water level, attitude, images, illumination, tension, etc. Therefore, the operation of the SLSS system also requires matching information with various sensors and actuators. The equipment designed in this study requires excellent adaptability and can be used for subsea pipelines with a maximum diameter of 762mm and a maximum bend angle of 15°, with minimal interference from sea conditions.

3. Method

3.1. Sealing theory, testing and simulation

There are numerous types of constitutive models for rubber, owing to the coexistence of hyperelasticity and viscoelasticity. Regarding the construction of constitutive models for each individual characteristic, the current approaches can be broadly categorized into three classes: phenomenological models, microstructure-based models, and hybrid models of the two. Among them, phenomenological models can be further divided into two types. One type is strain energy density function models expressed in terms of strain invariants. These models treat rubber elasticity by considering the deformation of rubber material as isotropic and uniform, thus representing the strain energy density function as a function of deformation tensor invariants, such as the Mooney-Rivlin model and the Yeoh model. The other type is strain energy function models expressed in terms of principal stretches, such as the Ogden model and the Marlow model.

The foam rubber extensively used in this mapping device differs from conventional rigid rubber in that it is prepared through a foaming process, resulting in a material with numerous voids. This characteristic allows its volume to decrease during compression, with the ability to regain its original shape upon pressure release. The Ogden model, most commonly employed for foam hyperelasticity, is utilized by current mainstream finite element simulation software. However, different software platforms use distinct nomenclatures for essentially the same model: Abaqus refers to it as the Hyperfoam model, COMSOL as the Storåkers model, and Ansys as the Ogden Foam model, although fundamentally identical.

When employing Abaqus' Hyperfoam model to characterize foamed EPDM rubber, it necessitates the specification of an appropriate Poisson's ratio to represent material volume changes during compression. The specific formula for the Hyperfoam model is:

$$U = \sum_{i=1}^{N} \frac{2\mu_i}{\alpha_i^2} \left[\hat{\lambda}_1^{\alpha_i} + \hat{\lambda}_2^{\alpha_i} + \hat{\lambda}_3^{\alpha_i} - 3 + \frac{1}{\beta_i} \left(\left(J^{e\ell} \right)^{-\alpha_i \beta_i} - 1 \right) \right] \tag{1}$$

where N is a material parameter, μ_i, α_i, β_i are temperature-dependent material parameters;

$$\hat{\lambda}_i = \left(J^{th} \right)^{-\frac{1}{3}} \lambda_i \quad \rightarrow \quad \hat{\lambda}_1 \hat{\lambda}_2 \hat{\lambda}_3 = J^{e\ell} \tag{2}$$

and λ_i are the principal stretches. The elastic and thermal volume ratios, $J^{e\ell}$ and J^{th}, are defined below.

The coefficients μ_i are related to the initial shear modules, μ_0, by

$$\mu_0 = \sum_{i=1}^{N} \mu_i \tag{3}$$

while the initial bulk modules, K_0, follow from

$$K_0 = \sum_{i=1}^{N} 2\mu_i \left(\frac{1}{3} + \beta_i \right) \tag{4}$$

For each term in the energy function, the coefficient β_i determines the degree of compressibility. β_i is related to the Poisson's ratio, v_i, by the expressions

$$\beta_i = \frac{v_i}{1 - 2v_i}, \quad v_i = \frac{\beta_i}{1 + 2\beta_i}. \tag{5}$$

Thus, if β_i is the same for all terms, we have a single effective Poisson's ratio, v. This effective Poisson's ratio is valid for finite values of the logarithmic principal strains ε_1, ε_2, ε_3; in uniaxial tension

$$\varepsilon_2 = \varepsilon_3 = -v\varepsilon_1 \tag{6}$$

Due to the non-homogeneous structure of the foam sealing rubber, which includes an outer layer of hard rubber reinforcement, accurate material parameters for simulation are obtained through stress-strain data acquisition based on compression experiments, as illustrated in Figure 6. Following the testing standard GB/T 18942.1-2003, a Zwick/Roell universal testing machine (Z020) is employed as the primary testing instrument (as shown in Figure 6(a)), operating in an environment of 6°C and 85% relative humidity. As depicted in Figure 6(b), cylindrical specimens are used for testing, with a total of five specimens tested and four valid datasets selected after eliminating significant deviations, corresponding to specimen thicknesses of 35.21mm, 34.63mm, 35.34mm, and 35.31mm. The testing machine, as shown in Figures 6(c) and (d), compresses the specimens vertically at a speed of 100mm/min, achieving compression levels of 70% or more.
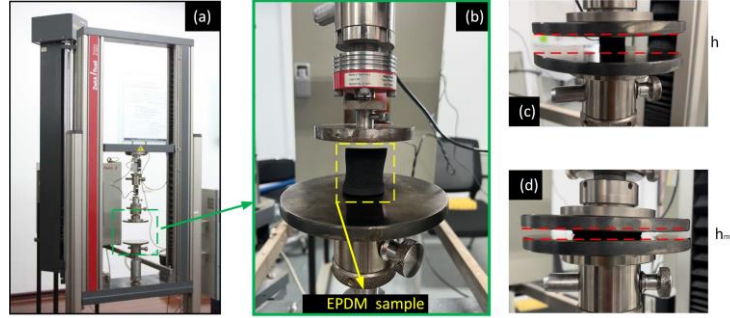

Fig. 6 Rubber compression test

The four valid testing curves are averaged to obtain the average stress-strain curve depicted in Figure 7(a). The compression process of the foam material can be understood as storing the work done by external forces as potential energy, with a small portion dissipated as heat. Computing the area under the stress-strain curve yields an index that characterizes the energy storage capacity per unit volume of the material, calculated as follows:

$$W = \int_0^{\varepsilon_{max}} \sigma d\varepsilon \qquad (7)$$

Where σ represents stress and ε represents strain, and integrating from initial deformation to maximum deformation yields the absorbed energy. The energy storage capacity corresponding to the stress-strain curve is illustrated in Figure 7(b). Due to the broad collapse platform exhibited by foam rubber during compression, it can absorb energy over a significant range of deformation. Moreover, as deformation approaches its limit, the structure becomes denser, leading to higher energy absorption per unit deformation.
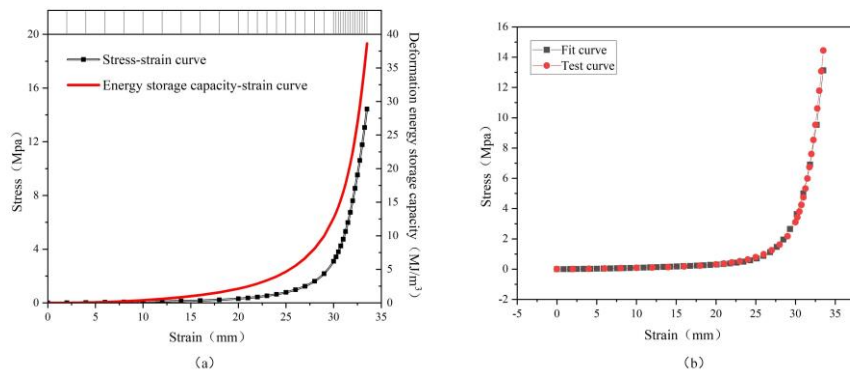

Fig. 7 Rubber compression test curve chart

The specific parameters obtained from evaluating the average of the test data using the hyperfoam model in the Abaqus software are presented in Table 1.

Table. 1 The specific parameters obtained from evaluate

Parameter	Value	Parameter	Value	Parameter	Value
μ_1	1.680e-3	μ_2	5.961e-20	μ_3	1.677e-03
α_1	2.80692	α_2	14.7774	α_3	-2.34955

6

β_1	7.83	β_2	7.83	β_3	7.83

The rubber sealing simulation model established in Abaqus software is illustrated in Figure 8. Hexagonal meshing is employed, characterized by strong element stiffness and relatively high computational accuracy. Each U-shaped steel component consisted of a total of 2000 units, with an approximate unit size of 5mm. Conversely, each foam EPDM rubber component comprised a total of 152750 units, with an approximate unit size of 2mm.
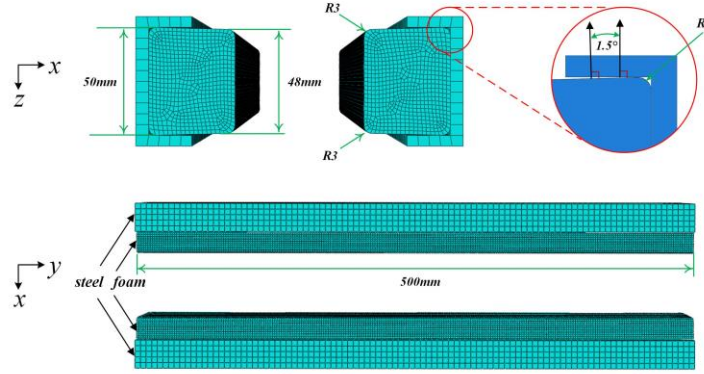

Fig. 8 Rubber sealing simulation model

Given the negligible deformation of the two U-steel components compared to the foam rubber, they were designated as rigid bodies. The penalty function model was utilized to describe each contact type, with a friction factor of 0.1 and isotropic directional settings. The simulation model was three-dimensional, with structural dimensions matching those of the actual materials used, as indicated in Figure 7 annotations.

3.2. Hyperbaric gas inflation theory

Due to the dry cabin operation basis of the mapping device, both the formation of the dry cabin and the discharge of water from the submarine's ballast tanks rely on hyperbaric gas inflation. Consequently, establishing a theoretical framework for hyperbaric gas inflation becomes particularly necessary, as it is crucial for optimizing and controlling the inflation process. Assuming that the outlet part of the air compressor is section 1, and its air supply pressure is p_1. The head height is Z_1. Gas outflow velocity is w_1. Assume that the entrance of the dry cabin is section 2. The air pressure in the dry cabin is p_2. The head height is Z_2. Gas outflow velocity is w_2. According to Bernoulli's equation:

$$Z_1 + \frac{p_1}{\gamma} + \frac{\alpha w_1^2}{2g} = Z_2 + \frac{p_2}{\gamma} + \frac{\alpha w_2^2}{2g} + h_w + \frac{1}{g}\int_{s_1}^{s_2}\frac{\partial w}{\partial t}ds \tag{8}$$

Where h_w is pipe loss, $\frac{1}{g}\int_1^2\frac{\partial w}{\partial t}ds$ is the inertial head. In the application of this project, the ratio of the gas supply pipe's sectional area to the tank's sectional area is far less than 0.1, so this item can be ignored. Then we can get:

$$h_w = (Z_1 - Z_2) + \frac{(p_1 - p_2)}{\gamma} + \frac{\alpha(w_1^2 - w_2^2)}{2g} \tag{9}$$

According to the Darcy–Weisbach equation, the calculation formula for pipeline loss h_w as follows:

$$h_w = h_f + h_j = \sum_{i=1}^n \lambda_i \frac{l_i}{d_i}\frac{w_i^2}{2g} + \sum_{i=1}^n \xi_i \frac{w_i^2}{2g} = w_1^2.LmdKs \tag{10}$$

Then:

$$Q_1 = A_1 W_1 = A_1\sqrt{\frac{h_w}{LmdKs}} \tag{11}$$

When the pressure in the tank forces the seawater to flow out of the drain hole, the flow coefficient is assumed to be μ, The sectional area of the orifice is S, and the equivalent head is H_0, then the outlet flow Q_p is:

$$Q_p = \mu S\sqrt{2gH_0} \tag{12}$$

Assuming the distance from the orifice to the liquid level is h', the distance from the orifice to the dry tank bottom is h, the atmospheric pressure is P, the distance from the dry tank bottom to the sea water level is H, and the internal pressure of the dry tank is P_2. The falling speed of the water surface is V_0. Sea water density is ρ_0, then the equivalent head H_0 is:

7

$$H_0 = H - h + h' + \frac{P_2 - P}{\rho_0 g} + \frac{V_0^2}{2g} \tag{13}$$

According to the continuous equation of fluid motion $Q_1 = Q_p$, the supply pressure and flow rate can be calculated, and the time required to discharge the subsea dry cabin under the supply pressure and flow rate can be calculated.

3.3. Structured light scanning principle and strategy

The structured light scanner used in this study utilized the principle of triangulation for mapping. As illustrated in Figure 9, in structured light triangulation, a laser emits a beam of light onto the surface of the object being measured, causing diffuse reflection. A portion of the reflected light is then converged by an imaging system at another angle, forming an image of the light spot on the built-in camera's photosensitive surface. A triangle is formed by the laser, the light spot, and the camera. The distance between the laser and the camera is precisely known, and the angle k between the light rays diffusely reflected to the camera and the laser emission line is also measurable by the system. Additionally, the angle ϕ between the camera's field of view (FOV) axis and the x-axis, as well as the angle $d\phi$ between the FOV axis and the laser reflected line, are known. Therefore, the angle between the reflected light ray and the y-axis, representing another internal angle of the triangle, can be determined. Consequently, the distance from the light spot to the scanner can be obtained.

$$d = \frac{l}{\sin k} \sin\left(\frac{\pi}{2} - \phi + d\phi\right) \cos\left(\frac{\pi}{2} + \phi - d\phi - k\right) \tag{14}$$
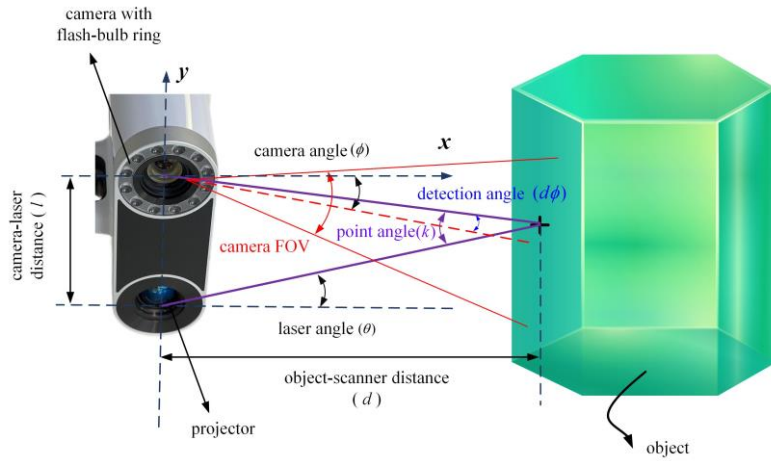

Fig. 9 Schematic diagram of the principle of structured light triangulation method

To enable remote control of the scanning process, an upper computer interface was designed as shown in Fig. 10. The upper computer interface is divided into several panels, among which those related to structured light scanning include the control panel responsible for switching the scanner's position within the dry cabin and the illumination and monitoring control panel. Other panels on the upper computer interface include controls for hydraulic cylinders and hydraulic winches, as well as displays for attitude, water depth, temperature, module status, and running status.

Fig. 10. Upper computer interface

8

The interface information and underwater sensor data are transmitted and displayed in real-time, providing crucial references for pipeline scanning. By inputting the motor's rotation count on the interface, accurate axial movement distance, circumferential rotation angle, and scanner swing angle can be obtained through gear ratio conversion. Based on the scanner's perspective and feedback of the scanning interface, the scanner's position within the dry cabin is controlled to achieve full coverage of the pipeline. This leads to the formulation of the scanning strategy depicted in Fig. 11.
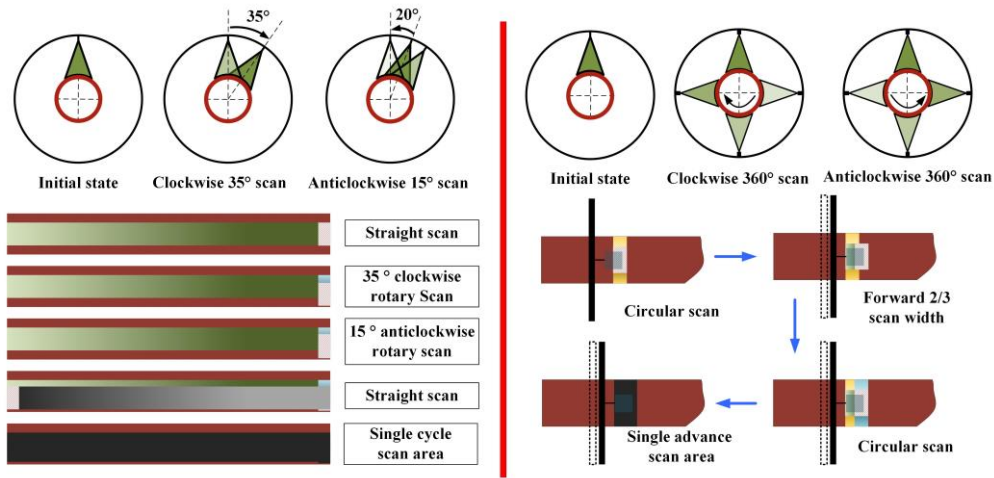
Fig. 11. Full coverage scanning strategy

According to the scanner's perspective and the requirement for the coverage rate of adjacent scans to be greater than 1/3, linear scanning and circular scanning methods are designed based on the size of the annular track. The linear scanning process, as shown on the left side of Fig. 11, involves first obtaining a single scan segment by moving straight, followed by clockwise rotation of 35° and counterclockwise rotation of 20° to enhance stitching success and ensure overlap to avoid data loss. Subsequently, the process repeats to acquire the second scan segment, and this cycle continues until 360° coverage of the pipeline surface is achieved. In contrast, circular scanning begins with circular scanning, followed by linear movement for the next circular scan, and this process repeats until full coverage scanning of the pipeline is completed.

4. Result and discussion

4.1. Sealing simulation results

The simulation results depicted in Figure 12 illustrate that as the rubber seal approaches closer to compression, the degree of compression increases. Concurrently, the pressure on the mating surface gradually intensifies. When the distance between the U-shaped steels reduces to zero, it is evident that the minimum pressure on the sealing surface surpasses the maximum operating water depth pressure requirement of 0.3 MPa.
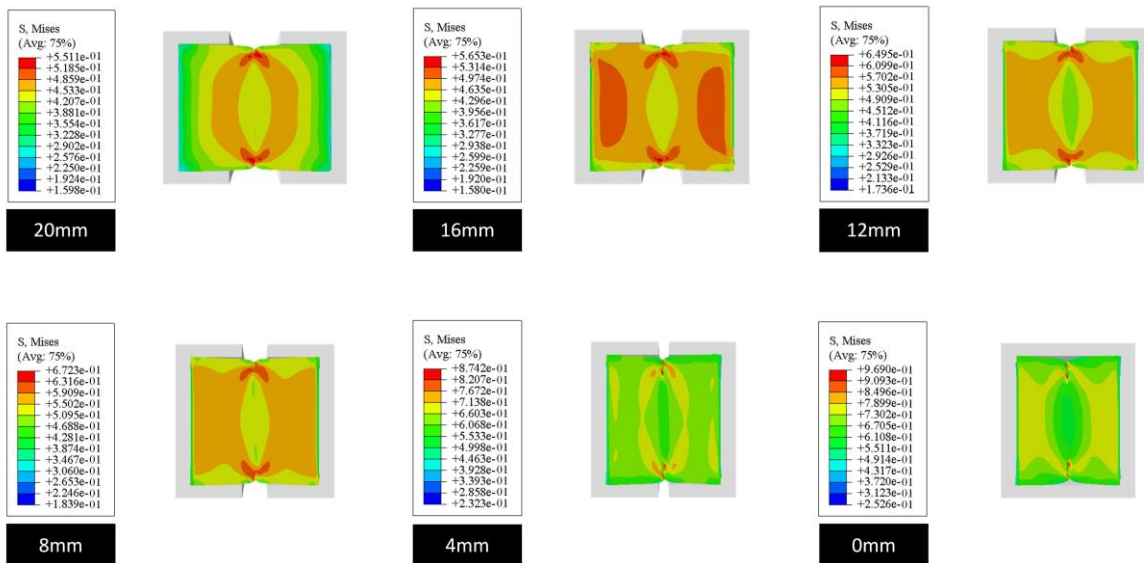

Fig. 12. Sealing simulation results

To better illustrate the pressure distribution, as depicted in Figure 13, pressure points on the sealing surface were extracted using Abaqus software and plotted as a distribution point line graph. It is observable that the minimum pressure is approximately 0.54 MPa, which is 1.8 times the designed water depth pressure. At the upper and lower ends of the sealing surface, stronger compression deformation occurs due

9

to the original angular structure of the rubber, forming two maximum pressure regions, termed "Max areas." Conversely, at the edges where significant deformation has not yet occurred, two minimum pressure regions, termed "Min areas," are present. As shown in Figure 12 (right), the Max and Min areas exhibit approximate symmetry about the center and are nearly equal in pressure magnitude.
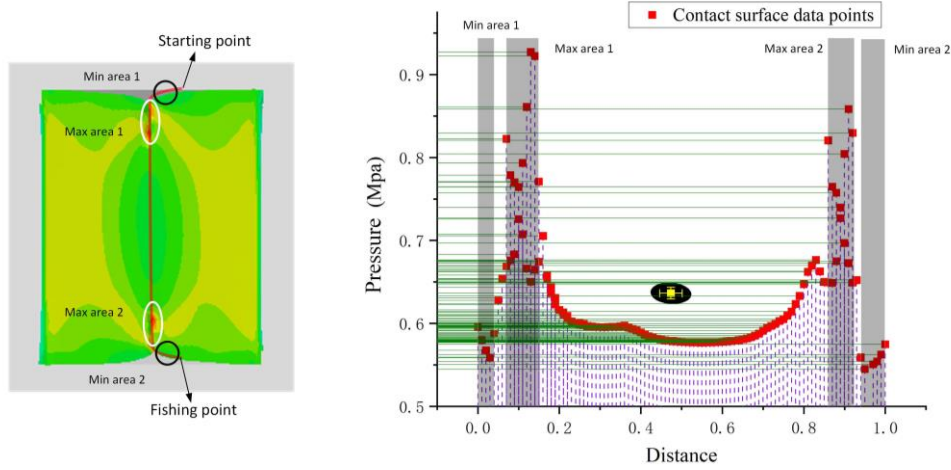

Fig. 13. Pressure distribution of docking sealing surface

Ignoring the presence of seawater and high-pressure air within the dry cabin, let's assume that the minimum contact stress on the sealing surface is $P_{\min}$, the operating water depth is H, corresponding to a water pressure of P_H. To ensure that seawater does not leak into the cabin from the lower end of the dry cabin, the minimum contact stress on the sealing interface must be greater than the pressure at the operating water depth. However, during the operation of the dry cabin, there is water inside the cabin and high-pressure air. Assuming the water level inside the cabin is h, corresponding to a water pressure of P_h, and the high-pressure air pressure inside the cabin is P_{air}, we can derive the following inequality:

$$P_H < P_h + P_{air} + P_{\min} \tag{15}$$

As mentioned earlier, ensuring that the external seawater pressure remains below the minimum contact pressure $P_{\min}$ on the sealing surface guarantees compliance with the design depth sealing requirements. However, regarding the pressure distribution on the sealing surface in this study, it is evident that high-pressure bands are actually formed at the upper and lower ends of the sealing surface. In an ideal scenario, this configuration could accommodate even greater operational water depths. Hence, as illustrated in Figure 14, a pressure distribution study of these data points was conducted within the Abaqus software. Specifically, four simulated mesh lines were selected at both the upper and lower ends for analysis.
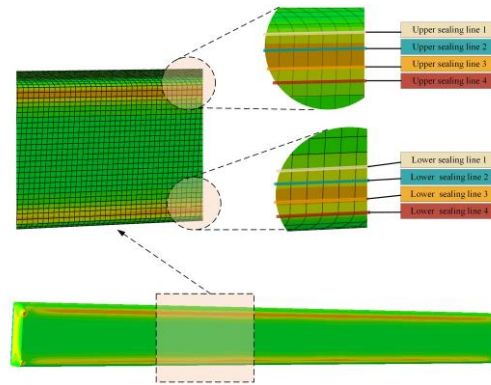

Fig. 14. Schematic diagram illustrating the selection of data points on the high-pressure sealing bands.

The pressure distribution plot generated from these points, as depicted in Fig. 14, reveals that the minimum pressure in this region is 0.61377 MPa. Compared to the conservative sealing determination method yielding 0.54 MPa, this represents a 13.6% improvement. Moreover, it is theoretically justified that individual low-pressure points cannot form leakage channels. Conversely, sparse high-pressure points cannot establish a stable sealing surface. As shown in Fig. 15, regions with a higher density of data points exhibit lower sealing pressures in the range of 0.65-0.75 MPa. Therefore, it is highly probable that the high-pressure bands at the upper and lower ends can seal against a water pressure of 0.65 MPa. At this point, the safety factor reaches 2.167. However, it is not advisable to adopt such a determination method in engineering design unless under exceptional circumstances.
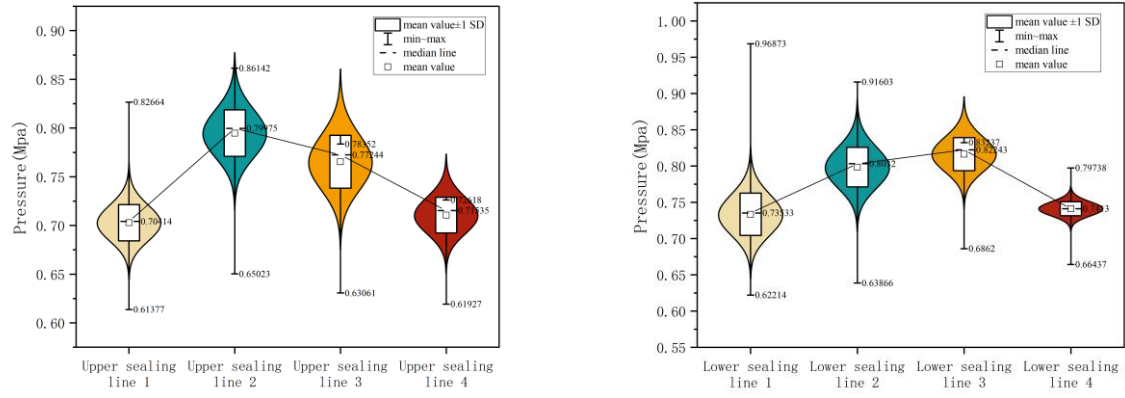
10

Fig. 15. Pressure distribution plot generated from these points

4.2. Hyperbaric gas blowing results

Fig 16 shows the monitoring of this project's underwater dry cabin evacuation process. The liquid level in the cabin decreases continuously under the action of pumps and high-pressure air (due to limitations of imaging conditions of monitoring equipment, the initial full water state is not visible), and the subsea pipelines are gradually exposed to the air in the cabin.
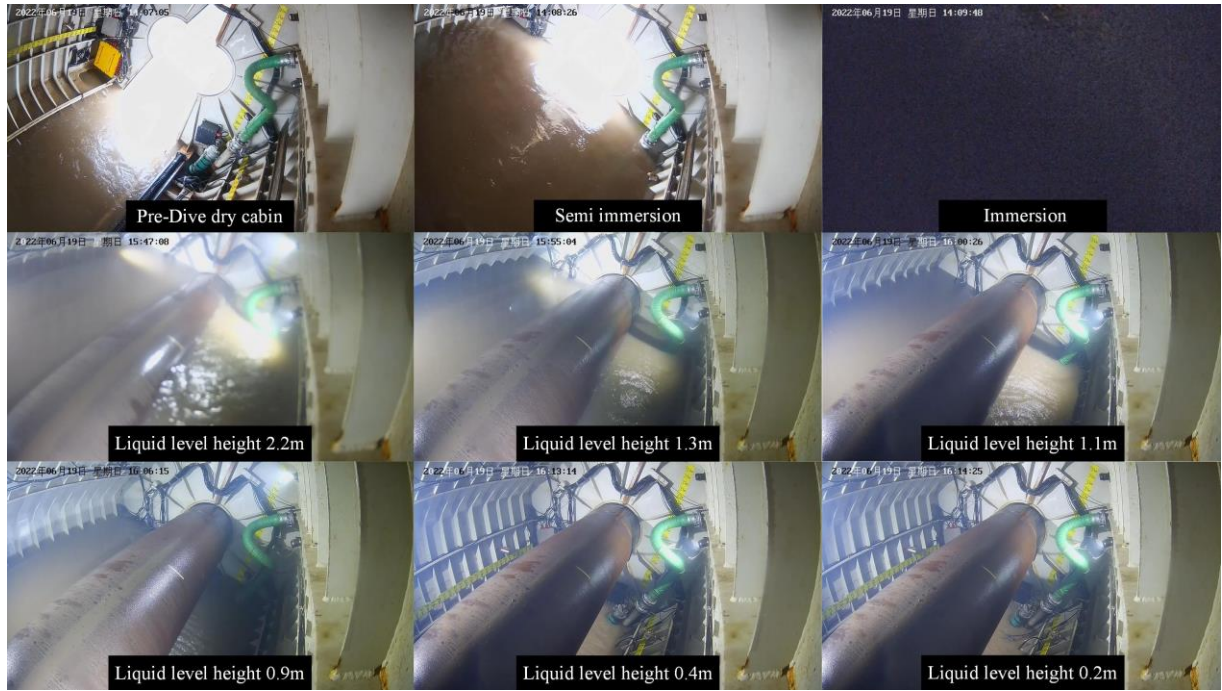

Fig. 16. Subsea dry cabin evacuation process monitoring

Figure 17 illustrates a time-dependent chart depicting the evacuation speed and total volume of the dry cabin over time. The evacuation speed exhibits non-constant behavior, initially peaking before gradually stabilizing at a lower rate. Subsequently, there is a notable surge in evacuation speed, ultimately returning to zero.

Analysis of the underlying principles reveals that the dry cabin's closed hexagonal structure, with its intake port positioned at the top, initially compresses high-pressure gas into a confined space, facilitating rapid drainage. However, as the cabin's air volume increases, the rise in gas pressure necessitates more time, resulting in a more gradual decline in the liquid level during the middle phase of evacuation. As the liquid level continues to decrease, the rate of volume change in the high-pressure gas slows down. Despite this, achieving liquid drainage still requires significant spatial displacement, thereby maintaining the evacuation speed at a relatively low level. During the sea trial, the activation of pumps (including submersible and pneumatic diaphragm pumps) expedites cabin drainage, notably enhancing evacuation speed during the final stage. Upon reaching the required water level for mapping purposes, the submersible pump is deactivated, leaving only the pneumatic diaphragm pump operational to sustain the water level. To ensure comprehensive protection of the dry cabin, high-pressure air is constantly supplied, despite the evacuation speed being zero at this point. The total drainage volume can be calculated by integrating the evacuation speed over time, as depicted by the trend in Figure 16 on the right.
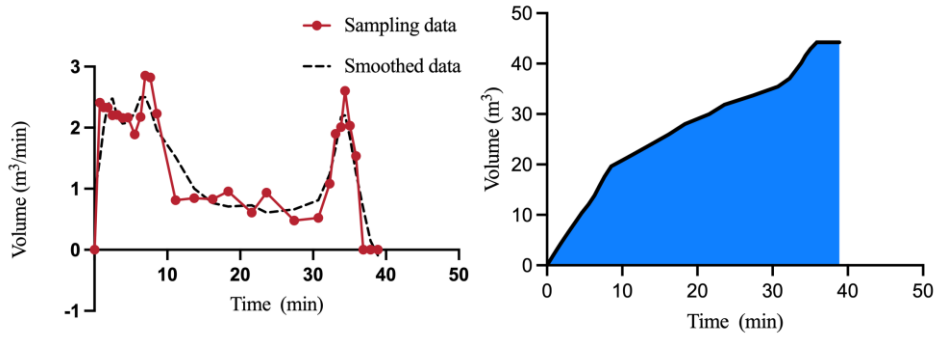
11

Fig. 17. Diagram of emptying rate versus time (left) and total drainage volume versus time (right)

4.3. Structured light mapping results

As depicted in Fig. 18(a), due to storage limitations and the nonlinear increase in data processing difficulty with data volume, a stepwise and segmented scanning approach was employed for the subsea pipeline. Each small segment underwent continuous scanning with a structured light scanner, and the scanning strategy was implemented as outlined in the preceding chapter. Image stitching between fragments was accomplished through feature matching, excluding partial bad point data and smoothing and filling in a small number of missing data. The resulting comprehensive 3D image, as illustrated in Fig. 18(b), faithfully portrays the true state of the tested subsea pipeline on the seafloor.

The structured light photometry's high precision enabled local magnification and a clear display of surface features, such as the weld seam on the pipeline shown in Fig. 18(c). Consequently, inspecting the entire pipe section facilitated the identification of hazardous points for further analysis and treatment, enabling the assessment of pipe damage, deformation, bending, and corrosion degrees.
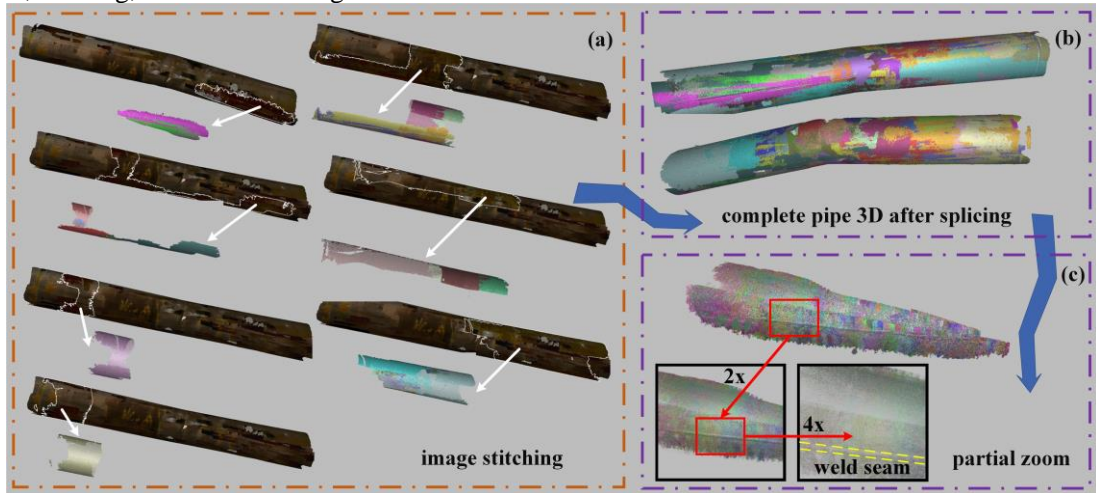

Fig. 17. Point cloud data stitching and detail enlargement

Structured light offers advantages in high-density data acquisition and extraction of multiple feature parameters unmatched by other techniques. The acquired data is quantifiable, editable, and can be interpolated, allowing extraction of bending angles at different distances along the pipeline and pipeline's axial lines, as depicted in Fig. 19 for the results of the subsea pipeline in this sea trial. Additionally, due to the structured light's extremely high accuracy, reaching up to 0.1mm precision, it achieves heights unattainable by conventional external inspection methods for pipeline defects.
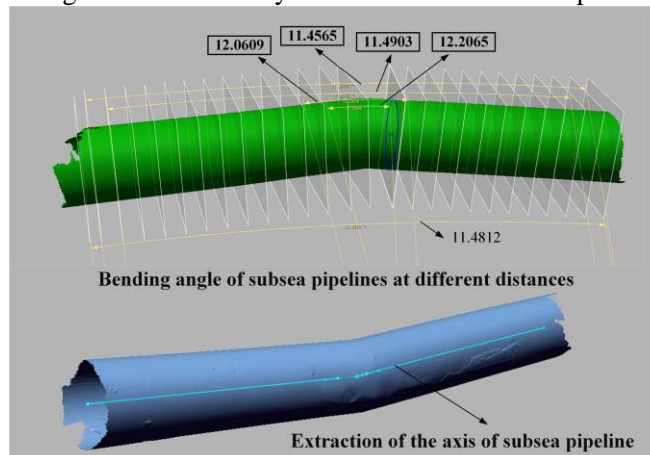

Fig. 19. Bending angle and axial line extraction diagram

5. Discussion

The present study introduces a significant innovation in subsea pipeline inspection by proposing a novel approach to detect defects using a dry cabin and structured light technology. This method aims to enhance pipeline scanning by mitigating seawater interference and harnessing the precision of structured light technology. Furthermore, the implementation of dry cabin technology for subsea pipelines in China represents a notable advancement, albeit with uncertainties to be addressed. Structured light technology, renowned for its high accuracy, finds widespread applications in various fields such as reverse engineering, quality inspection, biometric identification, and medical modeling. However, its application in subsea pipeline defect scanning is unprecedented globally, rendering this study innovative. This approach holds promise for improving subsea pipeline inspection through non-destructive testing capable of identifying various defects including cracks, dents, corrosion, and other damages.

Despite its potential benefits, the current project requires further refinement, particularly in the sealing structure of the dry cabin. Redesigning is imperative to minimize leaks and preserve the integrity of the high-pressure drainage effect. The existing sealing structure's limitations may compromise the dry environment and diminish the effectiveness of the pipeline scanning process. Exploring superior sealing methods or materials could enhance adaptability to larger pipeline defects.

Moreover, the driving structure for the structured light survey exhibits certain structural deficiencies, leading to operational issues such as poor performance and inadequate motor energy. Addressing these shortcomings is crucial to enhance the overall efficiency of the scanning process. Future studies should explore alternative driving structures and hydraulic driving methods to improve energy density and implement advanced motor control systems for real-time speed regulation and power distribution.

Furthermore, the reliance on manual input for the structured light scanner operation introduces inconvenience. To mitigate this limitation, leveraging real-time data quality discrimination to automate motor rotation through algorithmic means is proposed. This would facilitate automated scanning of subsea pipelines, thereby reducing potential hazards associated with human error. Enhancements in lighting, control programs, and other relevant aspects should be considered in future iterations.

Additionally, incorporating repair functions is essential for comprehensive subsea pipeline inspection and maintenance. Potential repair methods include welding, clamps, external wrapping with composite patches, and algorithm-driven adaptive structured light surveys. By integrating these functions, an efficient system can be developed for detecting, diagnosing, and repairing pipeline defects. In subsequent stages, research will focus on developing an integrated system for unmanned pipeline scanning and repair based on dry cabin technology. This will involve exploring key technologies such as flexible leak-proof sealing, precise medium replacement, automated pipeline scanning, and unmanned repair. Modular detection and repair tools based on dry cabins will be developed, paving the way for manned solutions for subsea pipeline repair to ensure safe and stable operation.

6. Conclusions

In conclusion, this paper introduces a novel approach for subsea pipeline defect mapping utilizing the subsea dry cabin and structured light scanning technology. The subsea dry cabin is established by expelling seawater from the underwater cabin using high-pressure gas in conjunction with submersible and diaphragm pumps, allowing for rapid scanning implementation within a short timeframe during slack-water conditions. Additionally, scanning strategies are devised within the constraints of the limited scanning radius and structured light scanner capabilities to ensure comprehensive coverage of the subsea pipeline surface.

The successful application of the subsea dry cabin for scanning expandable subsea pipelines in China represents a pioneering achievement, addressing numerous challenges associated with traditional subsea pipeline scanning techniques, such as measurement errors due to water flow, impurity interference, contact damage, and positioning difficulties. Furthermore, the utilization of structured light 3D scanning technology overcomes limitations inherent in other non-destructive testing (NDT) techniques, including restricted data information, small data samples, diminished accuracy, and high processing thresholds. The high precision, data editability, and versatile forms of structured light scanning data processing establish a robust foundation for its application in subsea pipeline defect scanning. Future research endeavors may extend the application of the subsea dry cabin and structured light scanning technology to diverse domains, encompassing ship hull inspection, pile foundation examination for offshore platforms, and offshore wind farm maintenance.

In summary, the amalgamation of the subsea dry cabin and structured light scanning technology presents a promising avenue for subsea pipeline defect scanning. This study showcases the feasibility and effectiveness of this approach while providing valuable insights into its application. This innovative methodology holds the potential to significantly enhance the accuracy, efficiency, and safety of subsea pipeline scanning, thereby contributing substantially to the maintenance and management of offshore infrastructure.

13

Compliance with ethics guidelines

References

[1]   Schofield C. Oceans: The blue frontier. Nature 2011;469:158–9. https://doi.org/10.1038/469158a.

[2]   Hai Z, Jia-wang C, Zi-qiang R, Pei-hao Z, Qiao-ling G, Xiao-ling L, et al. A new technique for high-fidelity cutting technology for hydrate samples. J Zhejiang Univ-Sci A 2022;23:40–54. https://doi.org/10.1631/jzus.A2100188.

[3]   Zhang B, Gong R, Wang T, Wang Z. Causes and Treatment Measures of Submarine Pipeline Free-Spanning. J Mar Sci Eng 2020;8:329. https://doi.org/10.3390/jmse8050329.

[4]   Chu J, Liu Y, Lv X, Li Q, Dong H, Song Y, et al. Experimental investigation on blockage predictions in gas pipelines using the pressure pulse wave method. Energy 2021;230:120897. https://doi.org/10.1016/j.energy.2021.120897.

[5]   Bai Y, Bai Q, editors. Ocean Engineering Series. Subsea Pipelines Risers, Oxford: Elsevier Science Ltd; 2005, p. ii. https://doi.org/10.1016/B978-008044566-3.50045-2.

[6]   Guo X, Nian T, Wang F, Zheng L. Landslides impact reduction effect by using honeycomb-hole submarine pipeline. Ocean Eng 2019;187:106155. https://doi.org/10.1016/j.oceaneng.2019.106155.

[7]   Lam KY, Zong Z, Wang QX. Dynamic response of a laminated pipeline on the seabed subjected to underwater shock. Compos Part B Eng 2003;34:59–66. https://doi.org/10.1016/S1359-8368(02)00072-0.

[8]   Meriem-Benziane M, Abdul-Wahab SA, Zahloul H, Babaziane B, Hadj-Meliani M, Pluvinage G. Finite element analysis of the integrity of an API X65 pipeline with a longitudinal crack repaired with single- and double-bonded composites. Compos Part B Eng 2015;77:431–9. https://doi.org/10.1016/j.compositesb.2015.03.008.

[9]   Hu X, Zhou C, Duan M, An C. Reliability analysis of marine risers with narrow and long corrosion defects under combined loads. Pet Sci 2014;11:139–46. https://doi.org/10.1007/s12182-014-0325-6.

[10]   Khan A, Ali SSA, Anwer A, Adil SH, Mériaudeau F. Subsea Pipeline Corrosion Estimation by Restoring and Enhancing Degraded Underwater Images. IEEE Access 2018;6:40585–601. https://doi.org/10.1109/ACCESS.2018.2855725.

[11]   Ben Seghier MEA, Mustaffa Z, Zayed T. Reliability assessment of subsea pipelines under the effect of spanning load and corrosion degradation. J Nat Gas Sci Eng 2022;102:104569. https://doi.org/10.1016/j.jngse.2022.104569.

[12]   Shi Y-M, Wang N, Gao F-P, Qi W-G, Wang J-Q. Physical modeling of the axial pipe-soil interaction for pipeline walking on a sloping sandy seabed. Ocean Eng 2019;178:20–30. https://doi.org/10.1016/j.oceaneng.2019.02.059.

[13]   Li Y, Shuai J, Jin Z-L, Zhao Y-T, Xu K. Local buckling failure analysis of high-strength pipelines. Pet Sci 2017;14:549–59. https://doi.org/10.1007/s12182-017-0172-3.

[14]   Ji H, Liu W, Yang K, Jiang J, Xing Z, Wang Y, et al. Physical model experiment on the influence of water depth on the underwater pipeline surface impacted by landslide surge. Sci Rep 2021;11:19301. https://doi.org/10.1038/s41598-021-98324-x.

[15]   Jia M, Li F, Zhang Y, Wu M, Li Y, Feng S, et al. The Nord Stream pipeline gas leaks released approximately 220,000 tonnes of methane into the atmosphere. Environ Sci Ecotechnology 2022;12:100210. https://doi.org/10.1016/j.ese.2022.100210.

[16]   Zhu H, Chen J, Lin Y, Guo J, Gao X, Chen Y, et al. In-Line Inspection (ILI) Techniques for Subsea Pipelines: State-of-the-Art. J Mar Sci Eng 2024;12:417. https://doi.org/10.3390/jmse12030417.

[17]   Chen W, Liu Z, Zhang H, Chen M, Zhang Y. A submarine pipeline segmentation method for noisy forward-looking sonar images using global information and coarse segmentation. Appl Ocean Res 2021;112:102691. https://doi.org/10.1016/j.apor.2021.102691.

[18]   Guan M, Cheng Y, Li Q, Wang C, Fang X, Yu J. An Effective Method for Submarine Buried Pipeline Detection via Multi-Sensor Data Fusion. IEEE Access 2019;7:125300–9. https://doi.org/10.1109/ACCESS.2019.2938264.

[19]   Zhang Y, Zhang H, Liu J, Zhang S, Liu Z, Lyu E, et al. Submarine pipeline tracking technology based on AUVs with forward looking sonar. Appl Ocean Res 2022;122:103128. https://doi.org/10.1016/j.apor.2022.103128.

[20]   Liling WANG, Guomin CAO, Yinshan DING, Tao ZAHNG, Kekuan WANG. Construction application of precise measurement technology on deformation of submarine pipelines based on pipeline clamp repair scheme. Pet Eng Constr 2023;49:8–12.

14

[21]   Ravanbod H. Application of neuro-fuzzy techniques in oil pipeline ultrasonic nondestructive testing. NDT E Int 2005;38:643–53. https://doi.org/10.1016/j.ndteint.2005.03.001.

[22]   She S, Chen Y, He Y, zhou Z, Zou X. Optimal design of remote field eddy current testing probe for ferromagnetic pipeline inspection. Measurement 2021;168:108306. https://doi.org/10.1016/j.measurement.2020.108306.

[23]   Peng X, Anyaoha U, Liu Z, Tsukada K. Analysis of Magnetic-Flux Leakage (MFL) Data for Pipeline Corrosion Assessment. IEEE Trans Magn 2020;56:1–15. https://doi.org/Design Issues and Challenges of Long-Range Ultrasonic.

[24]   Wang J, He R, Zhang H, Guo H, Wu Q. State-of-the-art Advancement and Development Direction of Submarine Pipeline Inspection Technology. China Pet Mach 2016;44:112–8. https://doi.org/10.16082/j.cnki.issn.1001-4578.2016.10.025.

[25]   Zhang S. High-speed 3D shape measurement with structured light methods: A review. Opt Lasers Eng 2018;106:119–31. https://doi.org/10.1016/j.optlaseng.2018.02.017.

[26]   Geng J. Structured-light 3D surface imaging: a tutorial. Adv Opt Photonics 2011;3:128–60. https://doi.org/10.1364/AOP.3.000128.

[27]   Daemen JHT, Loonen TGJ, Verhulst AC, Maal TJJ, Maessen JG, Vissers YLJ, et al. Three-Dimensional Imaging of the Chest Wall: A Comparison Between Three Different Imaging Systems. J Surg Res 2021;259:332–41. https://doi.org/10.1016/j.jss.2020.09.027.

[28]   Wu Z, Guo W, Zhang Q, Wang H, Li X, Chen Z. Time-overlapping structured-light projection: high performance on 3D shape measurement for complex dynamic scenes. Opt Express 2022;30:22467–86. https://doi.org/10.1364/OE.460088.

[29]   Ye J, Zhou C. Time-resolved coded structured light for 3D measurement. Microw Opt Technol Lett 2021;63:5–12. https://doi.org/10.1002/mop.32548.

[30]   Zhuo Z, Zhu C, Tang C-S, Xu H, Shi X, Mark V. 3D characterization of desiccation cracking in clayey soils using a structured light scanner. Eng Geol 2022;299:106566. https://doi.org/10.1016/j.enggeo.2022.106566.

[31]   Cui H, Liao W, Dai N, Cheng X. A flexible and rapid micro-adjustment algorithm for structured light 3D measurement system with camera–projector. Optik 2012;123:109–16. https://doi.org/10.1016/j.ijleo.2011.03.008.

[32]   Zhang K, Chermprayong P, Xiao F, Tzoumanikas D, Dams B, Kay S, et al. Aerial additive manufacturing with multiple autonomous robots. Nature 2022;609:709–17. https://doi.org/10.1038/s41586-022-04988-4.

[33]   Yueran PAN, Baofeng YANG. Design of Sealing Door of Dry Work Chamber with Normal Pressure Applied in Subsea Pipeline Repair. Pet Eng Constr 2016;42:46–9.

[34]   Wang K, Chen J, Huang J, Lin P, Guo J, Zhu H, et al. Investigation of dry environment construction Equipment's medium displacement system for submarine pipelines. Ocean Eng 2024;300:117365. https://doi.org/10.1016/j.oceaneng.2024.117365.